Atmos. Meas. Tech. Discuss., 6, 3983–4038, 2013
www.atmos-meas-tech-discuss.net/6/3983/2013/
doi:10.5194/amtd-6-3983-2013

Atmospheric Measurement Techniques Discussions

Daytime aerosol extinction profiles from the combination of CALIOP profiles and AERONET products

C. Marcos[1], R. Pedrós[1], J. L. Gómez-Amo[1,2], M. Sicard[3,4], M. P. Utrillas[1], C. Muñoz[3], A. Comerón[3], and J. A. Martinez-Lozano[1]

[1]Solar Radiation Group, Dep. Física de la Tierra y Termodinámica, Universitat de Valencia, Burjassot, Valencia, Spain
[2]Laboratory for Earth Observations and Analyses (UTMEA-TER), ENEA, Rome, Italy
[3]Remote Sensing Laboratory, Department of Signal Theory and Communications, Universitat Politècnica de Catalunya, Barcelona, Spain
[4]Institut d'Estudis Espacials de Catalunya – Aeronautics and Space Research Center (IEEC-CRAE), Universitat Politècnica de Catalunya, Barcelona, Spain

Received: 14 February 2013 – Accepted: 14 March 2013 – Published: 24 April 2013

Correspondence to: C. Marcos (carlos.marcos@uv.es)

Published by Copernicus Publications on behalf of the European Geosciences Union.

Abstract

The solar background illumination has a strong effect on CALIOP (Cloud-Aerosol Lidar with Orthogonal Polarization) measurements, leading to a decrease in the signal-to-noise ratio of the lidar signal. Because of this, CALIOP level 2 data algorithms might be limited in the retrieval of the properties of the aerosols in the atmosphere. In this work, we present a methodology that combines CALIOP level 1 data with AERONET (Aerosol RObotic NETwork) measurements to retrieve aerosol extinction profiles and lidar ratios in daytime conditions. In this way, we fulfill a two-fold objective: first, we obtain more accurate daytime aerosol information; second, we supplement column integrated measurements from AERONET sun photometers with information about the vertical distribution of aerosols. The methodology has been applied to Burjassot (39.30° N, 0.25° W) and Barcelona (41.39° N, 2.11° E) AERONET stations in the Mediterranean coast of Spain in the period from June 2006 to September 2011. We have found good agreement for the extinction profiles in several study cases of ground lidar measurements in Barcelona, coincident with CALIOP overpasses. Finally, the methodology has proved to be useful for the study of special episodes such as Saharan dust outbreaks.

1 Introduction

Atmospheric aerosols play an important role in the radiative balance of the earth-atmosphere system (IPCC, 2007). They can affect this balance in several ways: in a direct way, by scattering and absorbing radiation arriving from the Sun (Ramanathan et al., 2001); in an indirect way, acting as cloud condensation nuclei and modifying the optical properties and mean-life of clouds (Rotstayn and Penner, 2001); and in the so-called "semi-direct" way, changing the thermal structure of the atmosphere, which affects cloud formation (Ackerman et al., 2000).

To deal with the study of aerosols at a global scale, satellite-based sensors become essential since they perform worldwide measurements of the atmosphere. The great

AMTD
6, 3983–4038, 2013

majority of satellites that perform aerosol measurements only retrieve column integrated properties in cloud-free conditions. Amongst all the aerosol parameters measured by satellites, the most common are the aerosol optical depth (AOD) and the Ångström exponent (α), retrieved by sensors such as MODIS -Moderate Resolution Imaging Spectroradiometer (Remer et al., 2005), AVHRR – Advanced Very High Resolution Radiometer (Ignatov and Stowe, 2006), CERES – Clouds and the Earth's Radiant Energy System (Loeb and Kato, 2007), or AATSR – Advanced Along-Track Scanning Radiometer (Holzer-Popp et al., 2002).

Despite the usefulness of column integrated measurements, knowledge of the vertical distribution of aerosols is necessary to fully understand the total effect of aerosols in climate. Vertically-resolved data is needed to study the interactions between clouds and aerosols, essential for the estimation of the aerosol indirect effect, or the vertical structure of the atmosphere, for the determination of atmospheric dynamics or boundary layer structure (Penner, 2001).

Vertically-resolved measurements are usually performed by lidar (LIght Detection and Ranging) systems, which consist of active sensors that emit a laser beam to the atmosphere and are able to measure the signal backscattered by aerosols, clouds and molecules at different altitudes. Lidar raw data can be processed by different algorithms that allow us to retrieve aerosol extinction profiles at different wavelengths.

Since the 1990's several of these systems have been placed in orbit aboard spacecrafts. The first Lidar system in space was the LITE (Lidar In-space Technology Experiment) (LITE, 2011), developed by NASA and installed in the Discovery space shuttle from September the 9th to the September 20th in 1994. This mission was used as the base line for the subsequent Lidar systems in stable orbits, such as the GLAS (Geoscience Laser Altimeter System) aboard the ICESat – Ice, Cloud and land Elevation Satellite, 2004–2010 (ICESAT, 2011) or the CALIOP – Cloud-Aerosol Lidar with Orthogonal Polarization – sensor onboard the CALIPSO – Cloud-Aerosol Lidar and Infrared Pathfinder Satellite Observation – platform (CALIPSO, 2011; Winker et al., 2009), which was launched in April 2006 as a member of the A-Train satellite

AMTD
6, 3983–4038, 2013

constellation (ATRAIN, 2011). In particular, measurements from CALIOP are processed by a series of algorithms (Liu et al., 2005; Vaughan et al., 2005; Winker et al., 2006; Young et al., 2008) to obtain elaborated data, namely level 2 data, including extinction profiles and column aerosol optical depth at 532 and 1064 nm, in addition to aerosol classification products.

Several validation works show good agreement between CALIOP level 1 data and surface-based lidar measurements, although noticeable differences are found for altitudes below 3 km, which are attributed to aerosol spatial changes between the CALIOP overpass and the surface Lidar position (Mamouri et al., 2009; Mona et al., 2009; Pappalardo et al., 2010; Reba, 2010). However, comparisons of daytime level 2 data with AOD measurements from MODIS (Kittaka et al., 2011; Redemann et al., 2012) and AERONET (Bréon et al., 2011) show non-negligible discrepancies. Kacenelenbogen et al. (2011), in a detailed study of the CALIOP level 2 data limitations, point out some causes that would explain these results: low signal-to-noise ratio, failure in cloud removal or aerosol misclassifications.

In order to obtain more accurate aerosol profiles from satellite measurements over local areas, a synergy between CALIOP level 1 data and ground-based can be exploited. Examples of direct combination of CALIOP and sun-photometer measurements can be found in the works made by Kim et al. (2008), Chazette et al. (2009) or Chiang et al. (2011).

Kim et al. (2008) compare the extinction profiles obtained from the combination of CALIOP and sun photometer data with measurements made by a ground-based lidar over Seoul, Korea. For the only cloud-free daytime case, the lidar ratio from CALIOP and the ground-based lidar lied within the margin of error, and a mean difference of $0.02\,km^{-1}$ was found for the aerosol extinction coefficients. However, for the two cases affected by semi-transparent cirrus the lidar ratio could not be retrieved, and large discrepancies were found between CALIOP and ground-based measurements.

Chazette et al. (2009) analyze the ability of CALIOP to retrieve the aerosol optical properties in the lower troposphere in southeastern France, using CALIOP data from

AMTD
6, 3983–4038, 2013

version 2.01. The synergy between CALIOP and AERONET was exploited in two daytime cases, with moderate (~ 0.2) and low (< 0.1) AOD values respectively. In both cases the CALIOP inversion is able to find weak aerosols layers at altitudes where level 2 algorithms are unable. The authors conclude that this method is useful for obtaining information on the structure of aerosol layers for AOD values greater than 0.1.

In a comparison of CALIOP against ground-based lidar measurements over Chung-Li, Taiwan, Chiang et al. (2011) retrieved the lidar ratio for 16 cases combining satellite and ground-based photometer data. A mean lidar ratio of 23 ± 8 sr was found. The authors point that the aerosol variability and humidity may have an important effect in the discrepancies between ground-based lidar and CALIOP, and propose a solution for this based on the properties of aerosols in their local area.

According to these three precedent works, the combination of sun photometer and CALIPSO measurements during daytime is a useful technique for obtaining aerosol extinction profiles over a determined area. However, several factors limit the applicability of this method: low aerosol conditions, poor signal-to-noise ratio of CALIOP signal for some cases, presence of clouds or aerosol variability, both vertical and horizontal.

In this work we combine CALIOP level 1 data with AOD from surface sun photometers to study the aerosol vertical distribution of aerosol over the AERONET (AERONET, 2001) stations of Burjassot (39.51° N, 0.42° W) and Barcelona (41.39° N, 2.11° E) , in the Mediterranean coast of Spain. The results have been validated in a comparison with a ground-based lidar in Barcelona. Afterwards, the developed methodology has been applied to the stations of Burjassot and Barcelona in order to prove the validity of the CALIOP sensor for local-scale aerosol studies.

AMTD
6, 3983–4038, 2013

2 Instrumentation and measurements

2.1 CALIOP

The CALIOP sensor, the main instrument aboard the CALIPSO platform, is a Lidar system designed to perform measurements of the vertical profile of the atmosphere in near-nadir angle orbiting in a sun-synchronous orbit, 705 km from the earth surface. CALIOP has three operating channels: two operating at 532 nm, with parallel and perpendicular polarization respectively, and one at 1064 nm. However, only the total signal at 532 nm is used in this work.

Although CALIOP only offers aerosol information in the altitude range from −0.5 to 30 km, it also collects data at other altitudes that are used for the signal calibration and the calculation of the background noise caused by the solar radiation. This noise is one of the main problems that CALIOP has to deal with, especially in daytime measurements, when the noise can be similar to the signal itself, e.g. in clear atmospheres.

The main level 1 product offered by CALIOP is the attenuated backscatter (β'), defined at a height z and for a wavelength λ as:

$$\beta'_\lambda(z) = \beta_\lambda(z) \exp\left[-2 \int_z^{\mathrm{TOA}} \sigma_\lambda(r')\,\mathrm{d}r'\right] = \beta_\lambda(z) T^2_\lambda(z) \quad (1)$$

where β is the backscatter coefficient, σ is the extinction coefficient and T is the transmittance (Hostetler, 2006); and TOA is the top of the atmosphere height.

2.2 AERONET

AERONET (Holben et al., 1998) is a global network of sun photometer stations that carry out measurements of different aerosols properties. The instrument used in the AERONET network is the CIMEL 318A spectral radiometer, which is designed to perform spectral measurements (usually from 340 to 1020 nm) of the direct solar radiation

AMTD
6, 3983–4038, 2013

and the sky radiance at different angles. Using these measurements, and through an inversion algorithm (Dubovik and King, 2000) it is possible to retrieve information about the AOD, the phase function, the Ångström exponent and the size distribution.

The AERONET station of Burjassot (Fig. 1) is placed on the roof of the Physics Faculty, in the metropolitan area of Valencia (> 1.5 million inhabitants in 2011), 5 km far from Valencia city center and 10 km far from the Mediterranean Sea. The station is 30 m a.s.l. (above sea level) in a predominantly plain region, 15 km south of the nearest mountain range, with its highest peak at an altitude of 1000 m. The station has been supplying data to AERONET since April 2007.

The Barcelona site (Fig. 1) is located in the Universitat Politècnica de Catalunya (UPC), in the metropolitan area of Barcelona (> 3 million inhabitants in 2011), 5 km west of the city center and 6 km far from the Mediterranean coast. The sun photometer is placed 125 m a.s.l., at the foothill of Sierra de Collserola, at about 4 km far from its highest peak, the mount Tibidabo (512 m). This station has been operating since December 2004.

2.3 RSLAB lidar

The RSLAB Lidar is a Lidar system developed by the Remote Sensing Laboratory (RSLab) of the Universitat Politècnica de Catalunya (UPC). This system is part of the European Aerosol Research Lidar Network (EARLINET) that, among other duties, performs coincident measurements with CALIPSO overpasses for validation (Pappalardo et al., 2010).

At the time of the measurements (2008–2009) the lidar system measured the vertical profile at the elastic wavelengths of 532 and 1064 nm, the same as CALIOP, and at the Raman wavelength of 607 nm (Rocadenbosch et al., 2002). The lidar had an overlap distance of approximately 500 m, and a range resolution of 7.5 m, which effectively becomes a vertical resolution of 5.9 m due to the tilted position of the lidar system. In 2010, the system was upgraded to a 3-elastic wavelengths (355, 532 and 1064 nm) plus 3-Raman wavelengths (387, 407 and 607 nm) system (Reba et al., 2010). The

AMTD
6, 3983–4038, 2013

RSLab Lidar system is located next to the Barcelona AERONET station, so that the measurements made by both instruments are representative of the same aerosol conditions in the atmosphere.

3 Data processing

3.1 CALIOP

Due to the low signal-to-noise ratio in a single daytime level 1 profile, it is necessary to average a certain number of consecutive profiles to obtain a signal adequate enough to calculate the aerosol extinction profiles. In our method, we have averaged the level 1 signal over an area surrounding each AERONET station. This area must fulfill two requirements: being large enough to reduce the signal noise, but, at the same time, being small enough to represent the aerosol situation over each AERONET station.

Different criteria for the election of the averaging area can be found in other works where CALIOP and surface sun photometer data are combined. For example, depending on the case, the number of profiles averaged by Chazette et al. (2009) vary from 134 ($\sim$ 44 km) to more than 400 ($>$ 130 km). On the other hand, Kim et al. (2008) only use the 18 closest profiles ($\sim$ 6 km) to the ground-based lidar station.

The criterion we used to choose the averaging area is based on the one described by Ichoku et al. (2002) which estimate, using data from the TOMS (Total Ozone Mapping Spectrometer) sensor, that the mean speed of an aerosol front is about 50 km h^{-1}. Therefore the hourly averaged measurements of a sun photometer can apply to a 50 $\times$ 50 km window centered in the sun photometer. This averaging scale is similar to the one used by the CALIOP algorithms to detect aerosol layers.

To remove clouds from the level 1 profiles, we have used the CAD (Cloud-Aerosol discrimination) score, offered as part of the level 2 product catalogue (Liu et al., 2009). The CAD score presents negative values in those parts of the profile that the algorithm has classified as aerosol, and positive values for the parts classified as clouds.

AMTD
6, 3983–4038, 2013

The absolute value of this score is an estimate of the confidence of the classification. In addition to the CAD score, we have also used the Extinction Quality Control (QC) Flag 532 product that describes in which conditions the CALIOP algorithm has estimated the aerosol extinction profiles. We consider cloud-contaminated those profiles associated to CAD score values over −30 or with QC Flag values indicating that the initial assumptions of the algorithm had to be changed to avoid divergence or negative results. Those cases with more than 50 % of the profiles classified as cloud contaminated are then discarded.

After removing the cloudy profiles, a change in the vertical resolution is made from the original 30 m in level 1 data to 60 m. This change is made for two reasons: (1) to increase the signal-to-noise ratio; and (2) to match the vertical resolution of level 2 data for direct comparison. Finally, the uncertainty for the β' profiles, namely $\Delta\beta'$, is calculated as described by Liu et al. (2006).

3.2 AERONET

The CALIOP data used in this work are measured in the 532 nm channel. However, the AERONET sun photometers used in this work do not operate in that wavelength. The calculation of the AOD at 532 nm has been made by using the Ångström exponent, using the 675 and 500 nm channels when they are available (Burjassot since February 2009) or the 675 and 440 nm channels otherwise. We used the two nearest channels to 532 nm because the Ångström exponent can change with the wavelength (Martinez-Lozano et al., 1998). The Ångström law sets that the spectral variation of the AOD is given by:

$$\mathrm{AOD}_{\lambda_1} = \mathrm{AOD}_{\lambda_2} \left(\frac{\lambda_1}{\lambda_2}\right)^{-\alpha} \quad (2)$$

being λ_1 and λ_2 the selected wavelengths, and α the Ångström exponent. The values of the AOD obtained from AERONET measurements are averaged during one hour centered in the overpass of CALIPSO (Ichoku et al., 2002).

AMTD
6, 3983–4038, 2013

The uncertainty associated to the AOD at 532 nm has two major sources: the uncertainty in the measurement of the sun photometer and the temporal variability of the aerosols during the averaging time. In the AERONET webpage it is suggested that the measurements of the sun photometers have a typical uncertainty between 0.01 and 0.02, although it strictly changes with the solar height and wavelength (Estellés et al., 2006). Since the actual uncertainty at the CALIOP overpass time is likely to lie between the suggested values in the AERONET webpage (Estellés et al., 2006), we consider a mean constant uncertainty of 0.15 for all channels and then calculate the error at 532 nm with uncertainty propagation theory.

The uncertainty due to the variability of the AOD is calculated with Eq. (3):

$$\Delta AOD_{532}^{var} = \frac{AOD_{532}^{max} - AOD_{532}^{min}}{2} \quad (3)$$

where AOD_{532}^{max} and AOD_{532}^{min} are, respectively, the maximum and minimum values of AOD used in the average. Equation (3) is preferred to the standard deviation because the number of AERONET measurements during the averaging time is usually less than 5, and thus not relevant enough for a statistical analysis. Since the uncertainties caused by instrumental limitations and aerosol variability are independent, the total error for the AOD is calculated as:

$$\Delta AOD_{532} = \sqrt{\left(\Delta AOD_{532}^{ins}\right)^2 + \left(\Delta AOD_{532}^{var}\right)^2}. \quad (4)$$

3.3 RSLAB lidar

The RSLAB lidar signal is averaged one hour centered in the CALIPSO overpass over Barcelona, as it is done with the AERONET data. The aerosol extinction profiles are obtained using the two-component elastic lidar inversion algorithm (Fernald, 1984; Sasano and Nakane, 1984; Klett, 1985) and the AERONET AOD as a boundary condition (Reba, 2010). Once the extinction profile is calculated, its vertical resolution is changed so that it matches the CALIOP processed data vertical resolution (60 m).

AMTD
6, 3983–4038, 2013

4 Determination of extinction profiles

In our case, the extinction coefficients are calculated directly from β'. First, we separate the backscatter coefficient (β) and extinction (σ) coefficients into their respective components: gas molecules (m), aerosols (a) and ozone (o, which only contributes to extinction). This way, β' at 532 nm can be written as:

$$\beta'(z) = \left(\beta^{\mathrm{m}}(z) + \beta^{\mathrm{a}}(z)\right) \exp\left[-2\left(\int_{z}^{\mathrm{TOA}} \left(\sigma^{\mathrm{m}}(r') + \sigma^{\mathrm{o}}(r') + \sigma^{\mathrm{a}}(r')\right) \mathrm{d}r'\right)\right]. \quad (5)$$

If we consider the altitude increments (Δr) always positive, Eq. (5) can be written in a discrete form as:

$$\beta'_z = \left(\beta^{\mathrm{m}}_z + \mathrm{LR}\sigma^{\mathrm{a}}_z\right) \exp\left[-2\left(\sum_{i=1}^{z} \left[\left(\sigma^{\mathrm{m}}_i + \sigma^{\mathrm{o}}_i + \sigma^{\mathrm{a}}_i\right)|\Delta r_i|\right]\right)\right]. \quad (6)$$

From Eq. (6), σ^{a} at an altitude with index j can be analytically calculated using the Lambert W function (e.g. Veberič, 2012):

$$\sigma^{\mathrm{a}}_j = \left[-2\beta^{\mathrm{m}}_j|\Delta r_i| - \mathrm{LR}\cdot W\left\{-\frac{2\beta'_j|\Delta r_i|}{\mathrm{LR}} \exp\left(2\left(\mathrm{MOD}_j + \mathrm{OOD}_j + \mathrm{AOD}_{j-1}\right) - \frac{2\beta^{\mathrm{m}}_j|\Delta r_i|}{\mathrm{LR}}\right)\right\}\right] \cdot \left(2|\Delta r_i|\mathrm{LR}\right)^{-1} \quad (7)$$

where LR is the lidar ratio, and MOD_j and OOD_j stand for, respectively, the molecular and the ozone optical depth at an altitude of index j, and are defined as:

$$\mathrm{MOD}_z = \sum_{i=1}^{z} \left[\left(\sigma^{\mathrm{m}}_i\right)|\Delta r_i|\right] \quad (8)$$

$$\mathrm{OOD}_z = \sum_{i=1}^{z} \left[\left(\sigma^{\mathrm{o}}_i\right)|\Delta r_i|\right]. \quad (9)$$

AMTD
6, 3983–4038, 2013

Equation (7) has several unknowns required to determine σ^{a}. These terms are either measured (β') or obtained using models (β^{m}, MOD and OOD).

Finally, the solution of Eq. (7) requires a certain value of LR. In our case we consider a constant LR for the whole profile. This assumption is common in the inversion of elastic lidar signal and is adequate when the distribution of aerosols in the atmosphere is homogeneous (Kovalev, 1995). This constant LR will be iteratively determined so that the AOD from the CALIOP profile matches the AERONET AOD, with a maximum absolute difference of 0.015 (the instrumental error of the sun photometers).

Assuming a constant LR in the whole profile will unavoidably lead to a certain error if two or more aerosol layers with different LR co-exist in the atmosphere. However, using the AERONET AOD as a constraint allows us to avoid aerosol classifications that can be affected by daytime signal noise or imply wrong assignments of LR for some cases (Schuster, 2012).

Based on the typical values of LR measured by surface systems at 532 nm (Liu et al., 2002; Mattis et al., 2002; Ansmann et al., 2000; Franke et al., 2003), we have set a valid range for the LR between 20 and 110 sr. The cases not lying in this range will be discarded, since the exceptionally high or low values of LR suggest a non-negligible incompatibility of the measurements of CALIOP and AERONET, either because of aerosol variability, signal noise or failure in cloud removal.

Uncertainty calculations

An estimation of the uncertainty of the aerosol extinction profiles and LR has also been made using simulated profiles. The uncertainties due to the noise in CALIOP signal ($\Delta\sigma_{CAL}$ and ΔLR_{CAL}) are estimated by the following procedure:

1. At each altitude, a certain number of simulated backscatter coefficients are randomly generated assuming a normal distribution with a mean value of β' and a standard deviation equal to its associated uncertainty ($\Delta\beta'$).

AMTD
6, 3983–4038, 2013

2. For each simulated aerosol backscatter profile, an extinction profile together with a LR value is obtained, as it has been described in Sect. 3.2.

3. The uncertainty due to the noise in CALIOP signal is calculated as the standard deviation of these simulated aerosol extinction coefficients and LR values.

The uncertainties due to the AOD indetermination ($\Delta\sigma_{AOD}$ and ΔLR_{AOD}) are calculated in a similar way. The only difference is found in step 1, where random AOD values are generated following a normal distribution, instead of backscatter coefficients. Finally, the total uncertainty for both parameters is calculated as:

$$(\Delta\sigma) = \sqrt{(\Delta\sigma_{CAL})^2 + (\Delta\sigma_{AOD})^2} \quad (10)$$

$$(\Delta LR) = \sqrt{(\Delta LR_{CAL})^2 + (\Delta LR_{AOD})^2}. \quad (11)$$

A case study has been chosen for the determination of the optimal number of simulations. The low AOD in this case (0.055) makes it more sensitive to CALIOP signal noise and uncertainty in the AERONET measurements. The contribution to the total uncertainty in the LR (with a mean value of 69 sr and σ^a at 1 km (with a mean value of 0.020 km^{-1}) due to the AOD indetermination and CALIOP signal noise is shown in Fig. 2a and b. For a number of simulations greater than 300, variations in the uncertainty of both LR and σ^a are smaller than a 15 %, suggesting that this number of simulations is enough to get a good estimate of the uncertainties.

We can see that the main contribution to the uncertainty of the LR is the indetermination of the AOD. This is because the deviations of the simulated β' from the mean value are compensated in the whole profile. On the other hand, CALIOP signal noise is the main cause in the uncertainty of the σ^a values at a certain altitude.

AMTD
6, 3983–4038, 2013

5 Results

5.1 Summary

A summary of the number of CALIOP overpasses used in combination with AERONET from June 2006 to September 2011 is shown in Table 1. We can see that only a small percentage of the cases can be finally used to obtain valid aerosol extinction profiles. In 60 % of the cases, the CALIOP measurements have to be discarded due to the presence of clouds or the inability to find aerosols; and 15 % of the CALIOP overpasses cannot be exploited because there are no coincident AERONET measurements. Taking into account the time span in the database (more than 5 years), the number of valid cases is very limited. This is the drawback of using CALIOP data for a local study.

In Table 2 we present the mean values of the main parameters obtained with the suggested method (from now on, C + A, standing for CALIOP plus AERONET) and the level 2 data from CALIOP. The mean aerosol extinction profiles both for Burjassot and Barcelona have been calculated (see Fig. 3). As we can see, the aerosol layers reach, on average, a higher altitude in the case of Burjassot. This is caused by the Saharan dust intrusions, which have a bigger impact in the Burjassot station during the studied cases. More details on dust intrusions are given in Sect. 4.4. We also can see a noticeable discrepancy between the results obtained by C + A and the ones from the level 2 catalogue. For instance, the LR values obtained with C + A are systematically higher and have a greater variance than the ones given by level 2 data. This may be caused by the fact that in many cases CALIOP uses fixed values of LR, always under 70 sr, depending on the aerosol type. Finally, the mean LR values obtained in Barcelona, both for C + A and level 2 data, concur, within the margin of error, with the mean annual value of 55.5 sr retrieved by Sicard et al. (2011).

AMTD
6, 3983–4038, 2013

5.2 Comparison with RSLAB lidar

In this section, measurements of the RSLAB lidar are compared to the C + A method and CALIPSO level 2 extinction profiles. Three daytime cases are available for direct comparison, and each case is studied in detail in order to reach a better understanding of the capabilities and limits of the proposed C + A method and the level 2 data. The three available cases are called case a (10 August 2008), case b (22 March 2009) and case c (28 July 2009). More information about the CALIOP overpasses is given in Table 3.

The extinction profiles from RSLAB measurements are obtained by means of the the two-component elastic lidar inversion algorithm (Fernald, 1984; Sasano and Nakane, 1984; Klett, 1985), using a fixed value of AOD as a closing condition (Reba, 2010). Instead of using the column integrated AERONET-derived AOD, we use the C + A results to calculate the AOD over and under the overlap distance (dim 500 m) in each case, so we can have a better estimation of the actual aerosol load in the range the inversion is performed. In this way, comparisons between RSLAB, C + A and Level 2 data can be made more accurately. Finally, the vertical resolution of the RSLAB extinction profiles is changed from 5.9 to 60 m in order to match the resolution of C + A and level 2 data.

5.2.1 Comparison between RSLab and C + A

In this section we describe the three cases where comparisons between RSLab and C + A could be made. A summary of the results is shown in Table 4.

Case a (10 August 2008)

The AERONET-derived AOD for this case is 0.177 ± 0.017, while C + A estimates an AOD value of 0.12 above the overlap. The comparison between RSLAB and C + A is shown in Fig. 4. We can see that in both cases the aerosol layers reach the same altitude (~ 3 km), and that the C + A method is able to detect the weak ($< 0.025\ \mathrm{km}^{-1}$)

AMTD
6, 3983–4038, 2013

upper aerosol layer (2–3 km). Between 2 and 1.5 km, C + A reproduces the sharp variation in σ^a seen by RSLAB. Finally, for altitudes below 1.5 km, both RSLAB and C + A show that the values of σ^a fluctuate around 0.1 km^{-1}. The scatter plot shows a good correlation ($R^2 = 0.85$) between both cases, with a slope of 1.04. The LR retrieved by C + A has a value of 60 ± 6 sr, which is 18 sr bigger than the one obtained with the RSlab. This difference is three times bigger than the estimated uncertainty by C + A.

Case b (22 March 2009)

In this case, the AOD from AERONET has a value of 0.172 ± 0.019, and the estimated AOD over the overlap range is 0.13. In Fig. 5 a comparison between RSLab and C + A is shown. We can see that in this case most of the aerosols lie below 2 km, and that a sharp decrease in σ^a between 1 and 1.5 km is detected by both methods.

A good correlation is found between RSLab and C + A in this case ($R^2 = 0.93$), with a slope of 0.95. The C + A method has found a LR of 53 ± 5 sr, while RSlab-derived has a value of 44 sr, 9 sr fewer, a difference that is almost twice the estimated uncertainty.

Case c (28 July 2009)

This last case is the one with highest aerosol load, with an AOD of 0.228 ± 0.017 and an estimated AOD over the overlap range of 0.20. The aerosol profiles from RSLab and C + A are shown in Fig. 6. In the scatter plot we can see that the correlation between C + A and RSLab is higher for values of σ^a below 0.1 km^{-1}, which correspond to altitudes over 1.3 km, but decreases for bigger values of σ^a. The R^2 for the whole profile is found to be 0.71, and the linear fit has a slope of 0.88.

5.2.2 Comparison between RSLab and level 2 data

Before comparing RSLab and level 2 data we have to bear in mind that the RSLAB extinction profiles are obtained assuming a constant LR, while level 2 data make no restriction about it. Therefore, although the comparison is made for the three cases,

AMTD
6, 3983–4038, 2013

only case 2, where a constant LR is found by CALIOP algorithms, should be taken into account to assess the accuracy of level 2 extinction profiles. In this way we avoid the discrepancies that might be caused by the different assumptions made for obtaining the LR. The results of the comparisons can be seen in Table 5 and Fig. 7.

Case a (10 August 2008)

In Fig. 8 we show the aerosol classification scheme near the Barcelona station according to the level 2 *Feature Classification Flags*. It can be seen that three different aerosol situations (separated with dashed grey lines) lie within the averaging area (between red vertical lines): situation 1, with an upper layer classified as polluted dust (LR = 55 ± 22 sr) and a lower layer made of polluted continental (70 ± 25 sr) and polluted dust aerosols; situation 2, with three different layers of polluted dust, polluted continental and dust aerosols (40 ± 20 sr); and situation 3, consisting of a single layer of polluted dust that spreads from the ground to 2 km.

In Fig. 8 we can see the differences in the extinction profiles obtained with Level 2 data and RSLab. In both cases the sharp variation of σ^{a} is seen between 1.5 and 2 km. However, level 2 data fails in detecting the upper weak aerosol layers ($\sigma^{a} < 0.02\,\mathrm{km}^{-1}$) that C + A did notice.

Level 2 data underestimates the AOD in 0.02, which is a good estimation if we compare it with the average performance of level 2 against AERONET over Barcelona (Sect. 4.3). The RMSD is found to be 0.03, with a R^2 of 0.69. The mean LR for level 2 data is calculated as the aerosol extinction coefficients integrated for the whole profile, divided by the aerosol backscatter coefficients integrated for the whole profile:

$$\mathrm{LR}_{\mathrm{L2}} = \frac{\sum_{i=1}^{N} \sigma_i^{a}}{\sum_{i=1}^{N} \beta_i^{a}}. \quad (12)$$

AMTD
6, 3983–4038, 2013

For this case we have found a value of 55 sr, 13 sr bigger than the LR derived by RSLab.

Case b (22 March 2009)

The level 2 aerosol classifications (Fig. 9) show the existence of two main different aerosol situations within the averaging area, both consisting of polluted dust: the first one lying from the ground to 1 km; and the second reaching an altitude over 1.5 km. Figure 6 shows the different profiles obtained with RSLab and level 2 data.

Since only one type of aerosol has been detected, a direct comparison can be made with RSLab and C + A data (Table 6 and Fig. 10). We can see that for the studied parameters C + A show the best results, although level 2 data offers a reasonable good performance in this case: a difference in the AOD of 0.01, better than the mean performance of level 2 against AERONET over Barcelona (Sect. 4.3), a RMSD of 0.03 km^{-1} and a R^2 of 0.84. A LR of 55 sr has been found (corresponding to polluted dust), which is 11 sr greater than the LR obtained by the RSLab-photometer synergy.

Case c (28 July 2009)

According to level 2 data, there are two main different aerosol situations near the Barcelona station (Fig. 11): situation 1, consisting of a polluted dust layer going from the ground over 2 km; and situation 2, where dust and smoke aerosols (70 ± 28 sr) are detected within the polluted dust layer. The mean level 2 extinction profile within the whole averaging area are compared with the RSLAb measurements (Fig. 7). We can see the decrease in σ^a between 1 and 2.5 km in both cases, although level 2 data fails in detecting the upper aerosols with low σ^a ($< 0.025\ km^{-1}$). The level-2 derived AOD is found to be 0.19, 0.04 lower than the measured by AERONET, which is better than the mean performance of level 2 against AERONET over Barcelona (Sect. 4.3), a RMSD of 0.04 km^{-1} and a R^2 of 0.73. In this case the LR has a mean value of 57 sr, 15 sr higher than the LR found by the RSLab lidar.

AMTD
6, 3983–4038, 2013

5.2.3 Summary of the comparison

For case b, where discrepancies caused by the different assumptions of LR can be avoided, we have seen that C + A shows a better agreement with RSLab than level 2 data. For all cases, C + A shows good correlation with RSLab measurements. Moreover, the method could detect weak aerosol layers ($\sigma^a < 0.025\,km^{-1}$) at altitudes where level 2 algorithms could not. This fact is consistent with the results obtained by Sheridan et al. (2012), who find that for daytime conditions CALIOP algorithms are unable to detect aerosols with $\sigma^a < 0.02\,km^{-1}$ in a 50 % of the cases.

We have estimated RMSD values between 0.02 and 0.04 km^{-1}, which are consistent with the results obtained by Kim et al. (2008) for a cloud-free case with a mean difference of about 0.02 km^{-1}. However, big discrepancies have been found in the values of LR (between 9 and 20 sr), that have been overestimated for all cases.

Level 2 data has been compared to RSLab for the three cases, although we have to take into account that comparisons of cases a and c might be affected by the different assumptions made for obtaining the LR. For all cases the level 2 data overestimated the LR found by the RSLab between 11 and 15 sr. For the extinction profiles, the results obtained can be compared to those present in the work by Misra et al. (2012), where a similar comparison is made over Kanpur, India. For four cases where CALIPSO overpass distance is lower than 25 km, Misra et al. (2012) find a mean RMSD of 0.18 km^{-1} and a mean R^2 of 0.63 between level 2 data and a ground-based lidar plus a photometer. This is a poor performance compared to our results (Table 5), and can be explained by the difference of the AOD values over Kanpur (over 0.5) and Barcelona (under 0.25); or by the particularly good performance of level 2 data in the three cases studied over Barcelona, compared to the average results (Sect. 4.3).

5.3 Comparison between C + A and level 2 data

In Table 7 we present the results of the comparison between the AOD given by CALIOP level 2 data and the AOD from AERONET measurements (Fig. 12). The best results

AMTD
6, 3983–4038, 2013

are obtained for the Barcelona station, with lower values for both the mean difference (MD) and root mean squared difference (RMSD). It is remarkable that the estimated R^2 for the Barcelona station, 0.65, is much higher than the one obtained by Bréon et al. (2011), 0.4, comparing the CALIOP level 2 data against AOD measurements from AERONET. These differences may be explained by the fact that Bréon et al. (2011) used a square averaging window 150 km wide, which led to a greater aerosol variability influence, while in this work we use a much smaller circular area of radius of 25 km.

A comparison of the LR estimated by C + A and the ones given by level 2 data has been also made (Table 8). The LR for level 2 data is calculated in each case using Eq. (12). We can observe that the value for R^2 is less than 0.1 for all cases, which indicates a poor correlation between the LR obtained by C + A and CALIOP level 2 data. This may be caused by the fact that in many cases CALIOP uses pre-established fixed values for the LR, and because these values are never higher than 70 sr, although such LR values can actually be found (Liu et al., 2002; Mattis et al., 2002; Ansmann et al., 2000; Franke et al., 2003), for example for industrial, urban and biomass burning aerosols.

Finally, a comparison of σ^a is carried out. The main statistical parameters have been calculated for each profile, and their mean values are shown in Table 9. The mean values of R^2 obtained for all cases ($0.7 \sim 0.8$) indicates that, in general, there is a good correlation between C + A and level 2 data (Fig. 13). We find a mean RMSD of 0.06, which is equivalent to the mean value of σ at an altitude of 1.1 km in Burjassot or at 1.5 km in Barcelona.

5.4 Saharan dust outbreaks

Due to its proximity to Northern Africa, the Iberian Peninsula is usually affected by aerosol fronts arriving from the Saharan Desert (Pérez et al., 2006; Cachorro et al., 2008). To know the origin of the air masses we have used the HYSPLIT (HYbrid Single Particle Lagrangian Integrated Trajectory) back trajectories (Draxler and Rolph, 2003). We classified those cases as dust outbreaks when the back trajectories crossed the

AMTD
6, 3983–4038, 2013

Sahara Desert within the 5 previous days to the CALIPSO overpass. We have found 4 cases for the Burjassot station but none for Barcelona.

In Fig. 14 we show the mean aerosol extinction profiles for cases classified as dust outbreak and for the rest of cases. There is a noticeable difference between both situations: in cases affected by dust outbreaks aerosols reach an altitude of 6 km with an inhomogeneous vertical distribution, whereas the mean extinction profile for the rest of cases lies below 5 km and have an exponential shape.

We have obtained a mean LR of 56 sr for the dust outbreaks, with a standard deviation of 10 sr. These values are consistent with the ones retrieved by Pedrós et al. (2010), who obtained a LR between 55 ± 11 and 60 ± 6 sr (depending on the method) for Burjassot during dust outbreaks.

As a study case we present the dust outbreak on 1 August 2011, with an AERONET AOD of 0.476 ± 0.021 at 532 nm. The aerosol extinction profile, together with the back-trajectory analysis, is shown in Fig. 15.

Two different aerosol layers are noticed: one below 1500 m (red), and the other between 3000 and 6000 m (green). We have computed the back-trajectories for each layer (800 and 4500 m, respectively), and also for the aerosol free zone between them (2500 m). According to the results given by the HYSPLIT model, we can see that the air mass of the lowest layer had travelled near the land surface on the SE of the Iberian Peninsula, and that it raised to the altitude where it was detected about two days before the CALIOP overpass. For the aerosol-free zone between 1500 and 3000 m, the air masses travel from the Atlantic Ocean in a descending trajectory starting above 5000 m. Finally, we can see that the air masses at 4500 m come from the Western Sahara. They first travelled at the ground level and were advected later up to the altitude where they were detected in Burjassot.

In Fig. 16 we show the size distribution given by AERONET. It can be seen that the coarse mode (> 1 mum) is dominating, which indicates the presence of large particles, such as dust. The LR in this case is 61 ± 4 sr, consistent with the results of Pedrós et al. (2010).

AMTD
6, 3983–4038, 2013

Since this is a case where two clearly different aerosol layers co-exist, it is a good opportunity to study the divergences between C + A and level 2 data caused by the different methodology used for estimating the LR. In Fig. 17 we present the aerosol situation near Burjassot as seen by the CALIOP algorithms. The two layers are classified as dust (upper layer) and polluted dust (lower layer). In Table 10 we show the differences in the AOD and LR for the two layers and the whole profile for Level 2 and C + A data. We can see that level 2 AOD is clearly lower than the AERONET-derived AOD (0.232 vs. 0.477), a fact that might be caused by the inability to detect low σ^a values and the underestimation of the LR in one or both of the aerosol layers. It is also noticeable that the different methodology for estimating the LR has an effect on the relative vertical distribution of AOD, and the upper dust layer has a bigger weight in the total AOD for C + A (70 %) than for level 2 data (66 %).

6 Conclusions

We have developed a methodology for combining daytime data from CALIOP and AERONET for the determination of aerosol extinction profiles in local scales. In this way we try to fulfill a double objective: get more accurate extinction profiles than the ones given by CALIOP level 2 data and complete the column integrated information in AERONET sites with vertically-resolved data.

To prove the validity of the proposed methodology, we have applied it to the AERONET station of Barcelona, where the results can be compared to surface lidar measurements. Then, we have used this methodology for the study of aerosols over the AERONET station of Burjassot.

We have analyzed three cases where surface lidar measurements were made in coincidence with CALIOP overpasses. A mean RMSD of 0.03 km^{-1} with a correlation coefficient (R^2) of 0.8 has been obtained, which indicates a similar shape in the extinction profile. C + A has also been able to detect weak aerosol layers with $\sigma^a < 0.025\,km^{-1}$.

AMTD
6, 3983–4038, 2013

For case b (22 March 2009) C + A results show better agreement with RSLab than level 2 extinction profiles.

In the comparison with CALIOP and level 2 data, we have observed that the correlation between the AOD measurements varied depending on the AERONET station, obtaining better results for Barcelona, with a R^2 of 0.65. The lidar ratios obtained with the proposed methodology (namely, C + A) are greater than those given by CALIOP level 2 data, and show poor correlation ($R^2 < 0.1$). For the extinction profiles, a mean R^2 of 0.8 ± 0.2 has been found between CALIOP level 2 and C + A, which indicates a good agreement in the shape of the profiles.

With the help of the HYSPLIT model we could study the influence of the dessert aerosols over the Burjassot AERONET station. We have noticed relevant differences between the cases where air masses came from Northern of Africa and the rest of the cases, especially above 1500 m.

Acknowledgements. This research was funded by the Ministry of Science and Innovation (MICINN) of Spain through the projects CGL2009-07790 and CGL2011-13580, and by the Valencia Autonomous Government through the project PROMETEO-2010-064. The collaboration of C. Marcos was possible due to contract PROMETEO CI10-196 from the Valencia Autonomous Government. The authors gratefully acknowledge the Earth Sciences Division of the Barcelona Supercomputing Center for the use of the Barcelona AERONET sun photometer data, and the NOAA Air Resources Laboratory (ARL) for the provision of the HYSPLIT transport and dispersion model used in this publication. The CALIOP data used in this work were obtained from the NASA Langley Research Center Atmospheric Science Data Center.

References

Ackerman, A. S., Toon, O. B., Stevens, D. E., Heymsfield, A. J., Ramanathan, V., and Welton, E. J.: Reduction of Tropical Cloudiness by Soot, Science, 288, 1042–1047, doi:10.1126/science.288.5468.1042, 2000.

AERONET: http://aeronet.gsfc.nasa.gov/, last access: January 2013.

AMTD

6, 3983–4038, 2013

Ansmann, A., Althausen, D., Wandinger, U., Franke, K., Müller, D., Wagner, F., and Heintzenberg, J.: Vertical profiling of the Indian aerosol plume with six-wavelength lidar during INDOEX: A first case study, Geophys. Res. Lett., 27, 963–966, doi:10.1029/1999GL010902, 2000.

ATRAIN: http://atrain.nasa.gov/, last access: January 2013.

Bréon, F. M., Vermeulen, A., and Descloitres, J.: An evaluation of satellite aerosol products against Sunphotometer measurements, Remote Sens. Environ., 115, 3102–3111, doi:10.1016/j.rse.2011.06.017, 2011.

Cachorro, V. E., Toledano, C., Prats, N., Sorribas, M., Mogo, S., Berjón, A., Torres, B., Rodrigo, R., de la Rosa, J., and De Frutos, A. M.: The strongest desert dust intrusion mixed withsmoke over the Iberian Peninsula registered with Sun photometry, J. Geophys. Res., 113, D14S04, doi:10.1029/2007JD009582, 2008.

CALIPSO: http://www-calipso.larc.nasa.gov/about/payload.php, last access: January 2013.

Chazette, P., Raut, J.-C., Dulac, F., Berthier, S., Kim, S.-W., Royer, P., Sanak, J., Loaëc, S., and Grigaut-Desbrosses, H.: Simultaneous observations of lower tropospheric continental aerosols with a ground-based, an airborne, and the spaceborne CALIOP lidar system, J. Geophys. Res., 115, D00H31, doi:10.1029/2009JD012341, 2010.

Chiang, C.-W., Kumar Das, S., Shih, Y.-F., Liao, H.-S., and Nee, J.-B.: Comparison of CALIPSO and ground-based lidar profiles over Chung-Li, Taiwan, J. Quant. Spectrosc. Ra., 112, 197–203, doi:10.1016/j.jqsrt.2010.05.002, 2011.

Draxler, R. R. and Rolph, G. D.: HYSPLIT (HYbrid Single-Particle Lagrangian Integrated Trajectory) Model access via, NOAA ARL READY Website, http://www.arl.noaa.gov/ready/hysplit4.html (last access: January 2013), 2003.

Dubovik, O. and King, M. D.: A flexible inversion algorithm for retrieval of aerosol optical properties from Sun and sky radiance measurements, J. Geophys. Res., 105, 20673–20696, doi:10.1029/2000JD900282, 2000.

Estellés, V., Utrillas, M. P., Martínez-Lozano, J. A., Alcántara, A., Alados-Arboledas, L., Olmo, F. J., Lorente, J., de Cabo, X., Cachorro, V., Horvath, H., Labajo, A., Sorribas, M., Díaz, J. P., Díaz, A. M., Silva, A. M., Elías, T., Pujadas, M., Rodrigues, J. A., Cañada, J., and García, Y.:: Intercomparison of spectroradiometers and Sunphotometers for the determination of the aerosol optical depth during the VELETA2002 field campaign, J. Geophys. Res., 111, D17207, doi:10.1029/2005JD006047, 2006.

AMTD
6, 3983–4038, 2013

Estellés, V., Martínez-Lozano, J. A., and Utrillas, M. P.: The influence of air mass origin on the aerosol characteristics in Valencia, Spain, J. Geophys. Res., 112, D15211, doi:10.1029/2007JD008593, 2007.
Fernald, F.: Analysis of atmospheric lidar observations: some comments, Appl. Optics, 23, 652–653, 1984.
Franke, K., Ansmann, A., Müller, D., Althausen, D., Venkataraman, C., Reddy, M. S., Wagner, F., and Scheele, R.: Optical properties of the Indo-Asian haze layer over the tropical Indian Ocean, J. Geophys. Res., 108, 4059, doi:10.1029/2002JD002473, 2003.
Holben, B. N., Eck, T. F., Slutsker, I., Buis, J. P., Setzer, A., Vermote, E., Reagan, J. A., Kaufman, Y., Nakajima, T., Lavenu, F., and Smirnov, A.: AERONET – A federated instrument network and data archive for aerosol characterization, Remote Sens. Environ., 66, 1–16, 1968.
Holzer-Popp, T., Schroedter, M., and Gesell, G.: Retrieving aerosol optical depth and type in the boundary layer over land and ocean from simultaneous GOME spectrometer and ATSR-2 radiometer measurements, 1, Method description, J. Geophys. Res., 107, 4578, doi:10.1029/2001JD002013, 2002.
Hostetler, C. A., Liu, Z., Reagan, J., Vaughan, M., Winker, D., Hunt, W. H., Powell, K. A., and Trepte, C.: CALIOP Algorithm Theoretical Basis Document, Calibration and Level 1 Data Products, PC-SCI-201 Release 1.0, http://www-calipso.larc.nasa.gov/resources/project_documentation.php (last access: January 2013), 2006.
ICESAT: http://icesat.gsfc.nasa.gov/icesat/glas.php, last access: January 2013.
Ichoku, C., Shu, D. A., Mattoo, S., Kaufman, Y. J., Remer, L. A., Tanré, D., Slutsker, I., and Holben, B. N.: A spatio-temporal approach for global validation and analysis of MODIS aerosol products, Geophys. Res. Lett., 29, 12, doi:10.1029/2001GL013206, 2002.
Ignatov, A. and Stowe, L.: Aerosol retrievals from individual AVHRR channels, part I: retrieval algorithm and transition from Dave to 6 s radiative transfer model, J. Atmos. Sci., 59, 313–334, 2002.
IPCC: Climate Change 2007: The Physical Science Basis, in: Contribution of Working Group I to the Fourth Assessment Report of the Intergovernmental Panel on Climate Change, edited by: Solomon, S., Qin, D., Manning, M., Chen, Z., Marquis, M., Averyt, K. B., Tignor, M., and Miller, H. L., Cambridge University Press, Cambridge, UK and New York, USA, 2007.
Kacenelenbogen, M., Vaughan, M. A., Redemann, J., Hoff, R. M., Rogers, R. R., Ferrare, R. A., Russell, P. B., Hostetler, C. A., Hair, J. W., and Holben, B. N.: An accuracy assessment of the CALIOP/CALIPSO version 2/version 3 daytime aerosol extinction product based

AMTD
6, 3983–4038, 2013

on a detailed multi-sensor, multi-platform case study, Atmos. Chem. Phys., 11, 3981–4000, doi:10.5194/acp-11-3981-2011, 2011.
Kim, S.-W., Berthier, S., Raut, J.-C., Chazette, P., Dulac, F., and Yoon, S.-C.: Validation of aerosol and cloud layer structures from the space-borne lidar CALIOP using a ground-based lidar in Seoul, Korea, Atmos. Chem. Phys., 8, 3705–3720, doi:10.5194/acp-8-3705-2008, 2008.
Kittaka, C., Winker, D. M., Vaughan, M. A., Omar, A., and Remer, L. A.: Intercomparison of column aerosol optical depths from CALIPSO and MODIS-Aqua, Atmos. Meas. Tech., 4, 131–141, doi:10.5194/amt-4-131-2011, 2011.
Klett, J. D.: Lidar inversion with variable backscatter/extinction ratios, Appl. Optics, 24, 1638–1643, 1985.
Kovalev, V.: Sensitivity of the lidar solution to errors of the aerosol backscatter-to-extinction ratio: influence of a monotonic change in the aerosol extinction coefficient, Appl. Optics, 34, 3457–3462, 1995.
LITE: http://www-lite.larc.nasa.gov/, last access: January 2013.
Liu, Z., Sugimoto, N., and Murayama, T.: Extinction-to-backscatter ratio of Asian dust observed with high-spectral-resolution lidar and Raman lidar, Appl. Optics, 41, 2760–2767, 2002.
Liu, Z., Omar, A. H., Hu, Y., Vaughan, M. A., and Winker, D.: CALIOP Algorithm Theoretical Basis Document, Part 3: Scene Classification Algorithms, PC-SCI-202, http://www-calipso.larc.nasa.gov/resources/project_documentation.php (last access: January 2013), 2005.
Liu, Z., Hunt, W., Vaughan, M., Hostetler, C., McGill, M., Powell, K., Winker, D., and Hu, Y.: Estimating Random Errors Due to Shot Noise in Backscatter Lidar Observations, Appl. Optics, 45, 4437–4447, 2006.
Liu, Z., Vaughan, M., Winker, D., Kittaka, C., Getzewich, B., Kuehn, R., Omar, A., Powell, K., Trepte, C., and Hostetler, C.: The CALIPSO Lidar Cloud and Aerosol Discrimination: Version 2 Algorithm and Initial Assessment of Performance, J. Atmos. Ocean. Tech., 26, 1198–1213, doi:10.1175/2009JTECHA1229.1, 2009.
Loeb, N. G. and Kato, S.: Top-of-Atmosphere Direct Radiative Effect of Aerosols over the Tropical Oceans from the Clouds and the Earth's Radiant Energy System (CERES) Satellite Instrument, J. Climate, 15, 1474–1484, 2002.

AMTD
6, 3983–4038, 2013

Mamouri, R. E., Amiridis, V., Papayannis, A., Giannakaki, E., Tsaknakis, G., and Balis, D. S.: Validation of CALIPSO space-borne-derived attenuated backscatter coefficient profiles using a ground-based lidar in Athens, Greece, Atmos. Meas. Tech., 2, 513–522, doi:10.5194/amt-2-513-2009, 2009.

Martínez-Lozano, J. A., Utrillas, M. P., Tena, F., and Cachorro, V.: The parameterisation of the atmospheric aerosol optical depth using the Angstrom power law, Solar Energy, 63, 303–311, 1998.

Mattis, I., Ansmann, A., Müller, D., Wandinger, U., and Althausen, D.: Dual-wavelength Raman lidar observations of the extinction-to-backscatter ratio of Saharan dust, Geophys. Res. Lett., 29, 9, doi:10.1029/2002GL014721, 2002.

Misra, A., Tripathi, S. N., Kaul, D. S., Welton, E. J.: Study of MPLNET-Derived Aerosol Climatology over Kanpur, India, and Validation of CALIPSO Level 2 Version 3 Backscatter and Extinction Products, J. Atmos. Ocean. Tech., 29, 1285–1294, doi:10.1175/JTECH-D-11-00162.1, 2012.

Mona, L., Pappalardo, G., Amodeo, A., D'Amico, G., Madonna, F., Boselli, A., Giunta, A., Russo, F., and Cuomo, V.: One year of CNR-IMAA multi-wavelength Raman lidar measurements in coincidence with CALIPSO overpasses: Level 1 products comparison, Atmos. Chem. Phys., 9, 7213–7228, doi:10.5194/acp-9-7213-2009, 2009.

Pappalardo, G., Wandinger, U., Mona, L., Hiebsch, A., Mattis, I., Amodeo, A., Ansmann, A., Seifert, P., Linné, H., Apituley, A., Alados Arboledas, L., Balis, D., Chaikovsky, A., D'Amico, G., De Tomasi, F., Freudenthaler, V., Giannakaki, E., Giunta, A., Grigorov, I., Iarlori, M., Madonna, F., Mamouri, R. E., Nasti, L., Papayannis, A., Pietruczuk, A., Pujadas, M., Rizi, V., Rocadenbosch, F., Russo, F., Schnell, F., Spinelli, N., Wang, X., and Wiegner, M.: EARLINET correlative measurements for CALIPSO: First intercomparison results, J. Geophys. Res., 115, D00H19, doi:10.1029/2009JD012147, 2010.

Pedrós, R., Estellés, V., Sicard, M., Gómez-Amo, J. L., Utrillas, M. P., Martínez-Lozano, J. A., Rocadenbosch, F., Pérez, C., and Baldasano Recio, J. M.: Climatology of the aerosol extinction-to-backscatter ratio from Sun-photometric measurements, IEEE T. Geosci. Remote, 48, 237–249, doi:10.1109/TGRS.2009.2027699, 2010.

Penner, J. E., Zhang, S. Y., and Chuang, C. C.: Soot and smoke aerosol may not warm climate, J. Geophys. Res., 108, 4657, doi:10.1029/2003JD003409, 2003.

AMTD
6, 3983–4038, 2013

Pérez, C., Nickovic, S., Baldasano, J. M., Sicard, M., Rocadenbosch, F., and Cachorro, V. E.: A long Saharan dust event over the western Mediterranean: Lidar, Sun photometer observations, and regional dust modeling, J. Geophys. Res., 111, D15214, doi:10.1029/2005JD006579, 2006.

Ramanathan, V., Crutzen, P. J., Kiehl, J. T., and Rosenfeld, D.: Aerosols, Climate, and the Hydrological Cycle, Science, 294, 2119–2124, doi:10.1126/science.1064034, 2001.

Reba, M. N.: Data processing and inversion interfacing the UPC elastic-Raman lidar system, Tesis doctoral, Universitat Politècnica de Catalunya, España, 2010.

Redemann, J., Vaughan, M. A., Zhang, Q., Shinozuka, Y., Russell, P. B., Livingston, J. M., Kacenelenbogen, M., and Remer, L. A.: The comparison of MODIS-Aqua (C5) and CALIOP (V2 & V3) aerosol optical depth, Atmos. Chem. Phys., 12, 3025–3043, doi:10.5194/acp-12-3025-2012, 2012.

Remer, L. A., Kaufman, Y. J., Tanré, D., Mattoo, S., Chu, D. A., Martins, J. V., Li, R.-R., Ichoku, C., Levy, R. C., Kleidman, R. G., Eck, T. F., Vermote, E. and Holben, B. N.: The MODIS aerosol algorithm, products, and validation, J. Atmos. Sci., 62, 947–973, 2005.

Rocadenbosch, F., Sicard, M., Comerón, A., Baldasano, J. M., Rodríguez, A., Agishev, R., Muñoz, C. López, M. A., and García-Vizcaíno, D.: The UPC scanning raman lidar: an engineering overview. A: Twenty-first International Laser Radar Conference (ILRC21), in: Lidar Remote Sensing In Atmospheric and Earth Sciences, edited by: Bisonette, L. R., Gilles, R., and Vallée , G., Defence R & D Canada-Valcartier, 69–70, 2002.

Rotstayn, L. D. and Penner, J. E.: Indirect aerosol forcing, quasi forcing, and climate response, J. Climate, 14, 2960–2975, 2001.

Sasano, Y. and Nakane, H.: Significance of the extinction/backscatter ratio and the boundary value term in the solution for the two-component lidar equation, Appl. Optics, 23, 11–13, 1984.

Schuster, G. L., Vaughan, M., MacDonnell, D., Su, W., Winker, D., Dubovik, O., Lapyonok, T., and Trepte, C.: Comparison of CALIPSO aerosol optical depth retrievals to AERONET measurements, and a climatology for the lidar ratio of dust, Atmos. Chem. Phys., 12, 7431–7452, doi:10.5194/acp-12-7431-2012, 2012.

Sheridan, P. J., Andrews, E., Ogren, J. A., Tackett, J. L., and Winker, D. M.: Vertical profiles of aerosol optical properties over central Illinois and comparison with surface and satellite measurements, Atmos. Chem. Phys., 12, 11695–11721, doi:10.5194/acp-12-11695-2012, 2012.

AMTD
6, 3983–4038, 2013

Sicard, M., Rocadenbosch, F., Reba, M. N. M., Comerón, A., Tomás, S., García-Vízcaino, D., Batet, O., Barrios, R., Kumar, D., and Baldasano, J. M.: Seasonal variability of aerosol optical properties observed by means of a Raman lidar at an EARLINET site over Northeastern Spain, Atmos. Chem. Phys., 11, 175–190, doi:10.5194/acp-11-175-2011, 2011.

Vaughan, M. A., Winker, D. M., and Powell, K. A.: CALIOP Algorithm Theoretical Basis Document, Part 2: Feature Detection and Layer Properties Algorithms, PC-SCI-202 Part 2, Release 1.01, http://www-calipso.larc.nasa.gov/resources/project_documentation.php (last access: January 2013), 2005.

Veberič, D.: Lambert W function for applications in physics, Comput. Phys. Commun., 183, 2622–2628, doi:10.1016/j.cpc.2012.07.008, 2012.

Winker, D. M., Hostetler, C. A., Vaughan, M. A., and Omar, A. H.: CALIOP Algorithm Theoretical Basis Document, Part 1: CALIOP Instrument, and Algorithms Overview, PC-SCI-202 Part 1, Release 2.0, http://www-calipso.larc.nasa.gov/resources/project_documentation.php (last access: January 2013), 2006.

Winker, D. M., Vaughan, M. A., Omar, A., Hu, Y., Powell, K. A., Liu, Z., Hunt, W. H., and Young, S. A.: Overview of the CALIPSO Mission and CALIOP Data Processing Algorithms, J. Atmos. Ocean. Tech., 26, 2310–2323, doi:10.1175/2009JTECHA1281.1, 2009.

Young, S. A., Winker, D. M., Vaughan, M. A., Hu, Y., and Kuehn, R. E.: CALIOP Algorithm Theoretical Basis Document, Part 4: Extinction Retrieval Algorithms PC-SCI-202 Part 4, Release 1.0 – DRAFT, Last Update: 28 January 2008, http://www-calipso.larc.nasa.gov/resources/project_documentation.php (last access: January 2013), 2008.

AMTD
6, 3983–4038, 2013

Table 1. Summary of the valid and discarded cases. The mean value of the overpass times, minimum distance between CALIOP overpass and each AERONET station and number of averaged profiles is also shown. Numbers between brackets points the standard deviation of each parameter.

	Burjassot	Barcelona
Total cases	117	111
Cloudy and non-aerosol cases	68	74
No AERONET measurements	20	8
Not valid LR value	6	7
Valid cases	23	22
Overpass time (hh:mm)	13:20 (00:02)	13:08 (00:02)
Distance (km)	6 (3)	3 (2)
Averaged level 1 profiles	119 (19)	123 (19)

AMTD
6, 3983–4038, 2013

Table 2. Mean values for the AOD and LR. Standard deviation between brackets.

	Burjassot	Barcelona
	C + A	
AOD	0.19 (0.12)	0.17 (0.09)
LR (sr)	60 (16)	66 (13)
	CALIOP level 2	
AOD	0.12(0.08)	0.17 (0.13)
LR (sr)	48 (12)	53 (7)

AMTD
6, 3983–4038, 2013

Table 3. Summary of the CALIOP overpasses over Barcelona in the three study cases.

Case	a	b	c
Date	10 August 2008	22 March 2009	28 July 2009
$AOD_{(AERONET)}$	0.177 ± 0.017	0.172 ± 0.019	0.228 ± 0.017
Overpass time	13:08:06	13:11:41	13:10:30
Minimum distance (km)	6.0	2.1	4.6
Number of averaged profiles	115	118	141

AMTD
6, 3983–4038, 2013

Table 4. Results of the comparison between RSLAB and C + A for all cases. The studied parameters are root mean squared difference (RMSD), correlation coefficient (R^2), LR and $LR_x - LR_{RSlab}$ (ΔLR). The relative deviations with respect to the RSLab values are shown between brackets.

	Case a (10 August 2008)	Case b (22 March 2009)	Case c (28 July 2009)
RMSD	0.02	0.02	0.04
R^2	0.85	0.93	0.71
LR	60 ± 6	53 ± 5	62 ± 5
ΔLR	18 (40 %)	9 (20 %)	20 (48 %)

AMTD
6, 3983–4038, 2013

Table 5. Results of the comparison between RSLAB and level 2 data for all cases. The studied parameters are AOD, AOD_x-$AOD_{AERONET}$(ΔAOD), root mean squared difference (RMSD), correlation coefficient (R^2), mean LR ($\overline{LR}$) and $\overline{LR}_x - LR_{RSlab}$($\Delta LR$). The relative deviations with respect to the RSLab values are shown between brackets.

	Case a (10 August 2008)	Case b (22 March 2009)	Case c (28 July 2009)
AOD	0.16	0.18	0.19
ΔAOD	−0.02 (−10 %)	0.01 (6 %)	−0.04 (17 %)
RMSD	0.03	0.03	0.04
R^2	0.69	0.84	0.73
$\overline{LR}$ (sr)	55	55	57
ΔLR (sr)	13 (42 %)	11 (25 %)	15 (35 %)
Constant LR	No	Yes	No

AMTD
6, 3983–4038, 2013

Table 6. Results of the comparison between RSLAB and C + A and level 2 for case b. The studied parameters AOD, AOD_x-$AOD_{AERONET}$ (ΔAOD), root mean squared difference (RMSD), correlation coefficient (R^2), mean LR ($\overline{LR}$) and $\overline{LR}_x - LR_{RSlab}$ (ΔLR). The relative deviations with respect to the RSLab values are shown between brackets.

	RSLab	C + A	Level 2
AOD	0.172	0.172	0.183
ΔAOD	–	–	0.010 (6 %)
RMSD	–	0.025	0.033
R^2	–	0.93	0.84
$\overline{LR}$ (sr)	44	53 ± 5	55
ΔLR (sr)	–	9 (20 %)	11 (25 %)

AMTD
6, 3983–4038, 2013

Table 7. Mean AOD values given by AERONET and CALIOP level 2 data, with the standard deviations between brackets. Statistical parameters from the comparison are also shown: mean difference (MD), root mean squared difference (RMSD), correlation coefficient (R^2), and percentage of AOD in the estimated margin of error (1Δ).

	Burjassot	Barcelona	Total
$\overline{\text{AOD}}_{\text{AERONET}}$	0.19 (0.12)	0.17 (0.09)	0.18 (0.10)
$\overline{\text{AOD}}_{\text{N2}}$	0.12 (0.09)	0.17 (0.13)	0.14 (0.11)
MD	0.06	0.006	0.04
RMSD	0.11	0.07	0.09
R^2	0.5	0.7	0.5
1Δ (%)	9	14	12

AMTD
6, 3983–4038, 2013

Table 8. Mean LR values from C + A and CALIOP level 2 data, with the standard deviations between brackets. Statistical parameters from the comparison are also shown: mean difference (MD), root mean squared difference (RMSD), correlation coefficient (R^2), and percentage of AOD in the estimated margin of error (1Δ).

	Burjassot	Barcelona	Total
$\overline{LR}_{C+A}$	60 (16)	66 (12)	63 (15)
$\overline{LR}_{N2}$	48 (12)	55 (13)	51 (10)
MD	9	13	11
RMSD	18	19	19
R^2	0.03	0.002	0.03
1Δ (%)	16	31	23

AMTD
6, 3983–4038, 2013

Table 9. Mean values of the statistical parameters obtained from σ^a case-to-case comparisons: mean difference (MD), root mean squared difference (RMSD), correlation coefficient (R^2), and percentage of AOD in the estimated margin of error (1Δ).

	Burjassot	Barcelona	Total
MD	0.014 (0.024)	0.005 (0.003)	0.01 (0.03)
RMSD	0.06 (0.03)	0.06 (0.04)	0.06 (0.03)
R^2	0.7 (0.3)	0.8 (0.2)	0.8 (0.2)
1Δ (%)	13 (8)	9 (5)	11 (7)

AMTD
6, 3983–4038, 2013

Table 10. AOD and LR from Level 2 data and C + A for 1 August 2011 over Burjassot. Values between brackets show the relative contribution to the total AOD.

		Level 2	C + A
AOD	Upper layer	0.153 (66 %)	0.333 (70 %)
	Lowe later	0.079 (34 %)	0.143 (30 %)
	Total	0.232	0.477
LR (sr)	Upper layer	40	61
	Lowe later	55	61
	Mean	44	61

AMTD
6, 3983–4038, 2013

Fig. 1. Location of Barcelona and Burjassot AERONET sites. The circle around each station shows the actual size of the averaging area.

AMTD
6, 3983–4038, 2013

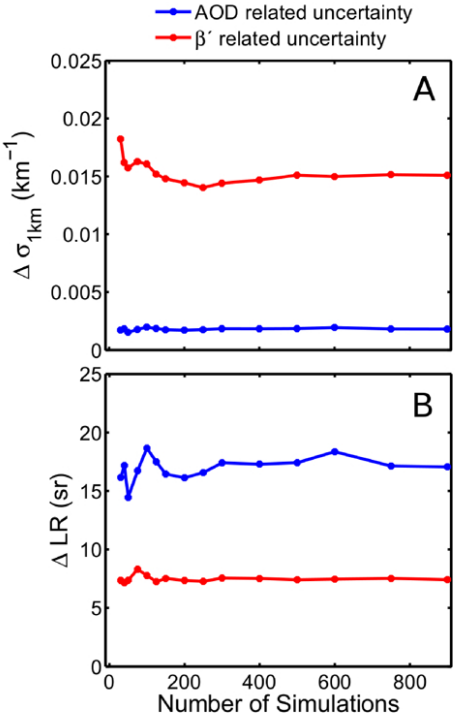

Fig. 2. (A) Estimated uncertainty for σ^a at 1 km and **(B)** estimated uncertainty for LR at against number of simulated profiles. The blue line shows the contribution of the uncertainty in AOD and the red line the contribution of the CALIOP noise.

AMTD
6, 3983–4038, 2013

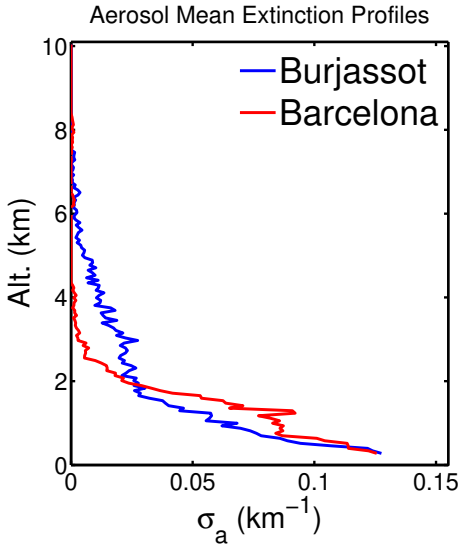

Fig. 3. Mean aerosol extinction profiles for the Barcelona (red line) and Burjassot (blue line) sites.

AMTD
6, 3983–4038, 2013

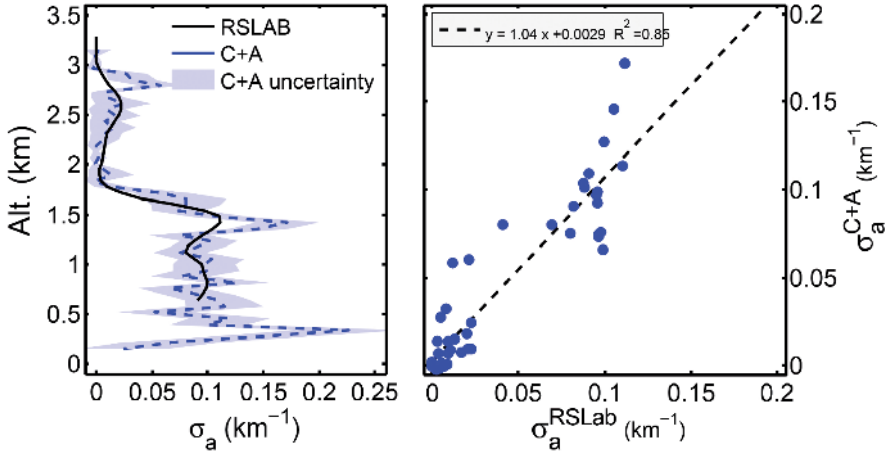

Fig. 4. Left panel: aerosol extinction profiles from RSLAB (black line) and C + A (blue dashed line) for case a (10 August 2008). Right panel: σ^a from C + A vs. σ^a from RSLab. The black dashed line shows the linear fit.

AMTD
6, 3983–4038, 2013

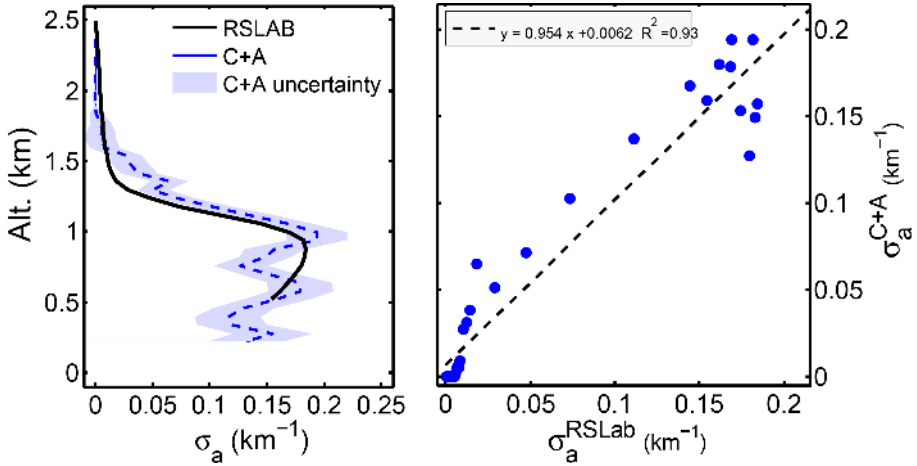

Fig. 5. Left panel: aerosol extinction profiles from RSLAB (black line) and C + A (blue dashed line) for case b (22 March 2009). Right panel: σ^a from C + A vs. σ^a from RSLab. The black dashed line shows the linear fit.

AMTD
6, 3983–4038, 2013

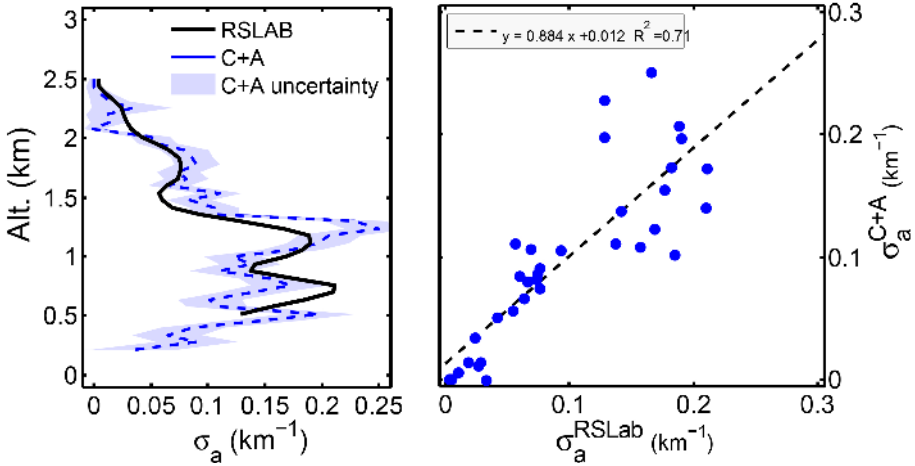

Fig. 6. Left panel: aerosol extinction profiles from RSLAB (black line) and C + A (blue dashed line) for case c (28 July 2009). Right panel: σ^a from C + A vs. σ^a from RSLab. The black dashed line shows the linear fit.

AMTD
6, 3983–4038, 2013

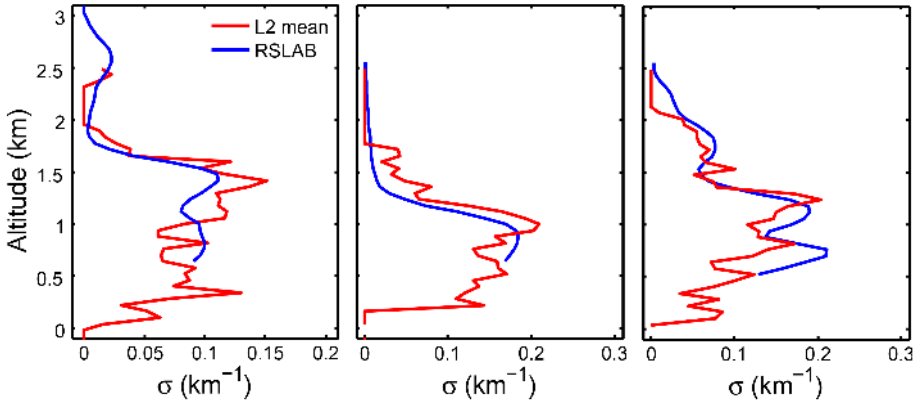

Fig. 7. Aerosol extinction profiles from RSLAB (blue line) and Level 2 (red line) for all cases.

AMTD
6, 3983–4038, 2013

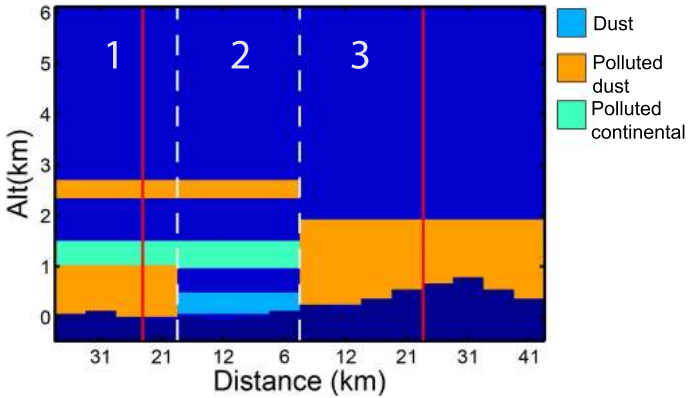

Fig. 8. Aerosol classification for case a (10 August 2008) according to CALIPSO level 2 data. The x-axis show the distance of the classification profiles from the Barcelona station. Red lines point the averaging area limits, and grey dashed lines delimit the three different aerosol situations (1, 2 and 3).

AMTD
6, 3983–4038, 2013

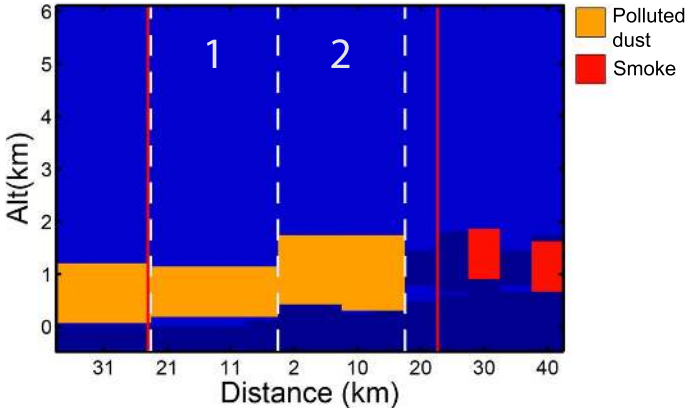

Fig. 9. Aerosol classification for case *b* (22 March 2009) according to CALIPSO level 2 data. The x-axis show the distance of the classification profiles from the Barcelona station. Red lines point the averaging area limits, and grey dashed lines delimit the two different aerosol situations (1 and 2).

AMTD
6, 3983–4038, 2013

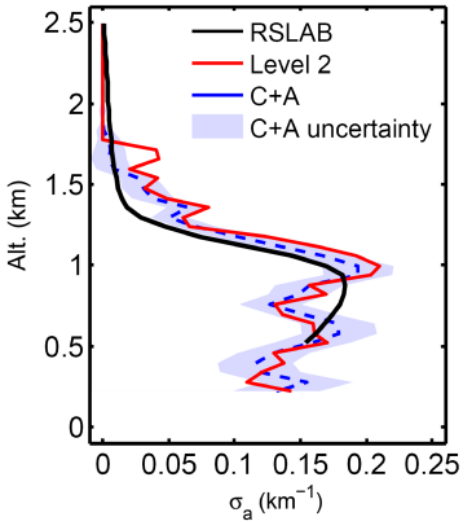

Fig. 10. Aerosol extinction profile for case b (22 March 2009) from RSLab lidar (black line), Level 2 data (red line) and C + A (blue dashed line).

AMTD
6, 3983–4038, 2013

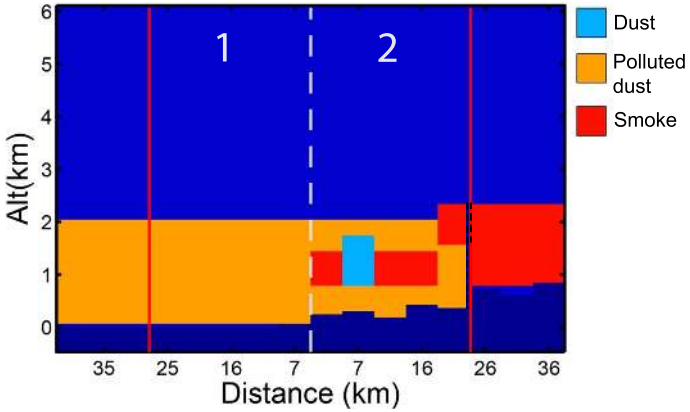

Fig. 11. Aerosol classification for case b (28 July 2009) according to CALIPSO level 2 data. The x-axis show the distance of the classification profiles from the Barcelona station. Red lines point the averaging area limits, and grey dashed lines delimit the two different aerosol situations (1 and 2).

AMTD
6, 3983–4038, 2013

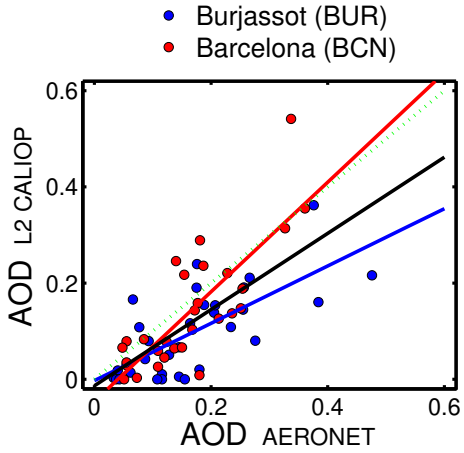

Fig. 12. CALIOP level 2 AOD vs. AERONET derived AOD at 532 nm. Blue dots are the measurements over the Burjassot site and the red dots over Barcelona. The blue and the red lines show, respectively, the linear fits for Burjassot and Barcelona and the black line is the linear fit for all measurements.

AMTD
6, 3983–4038, 2013

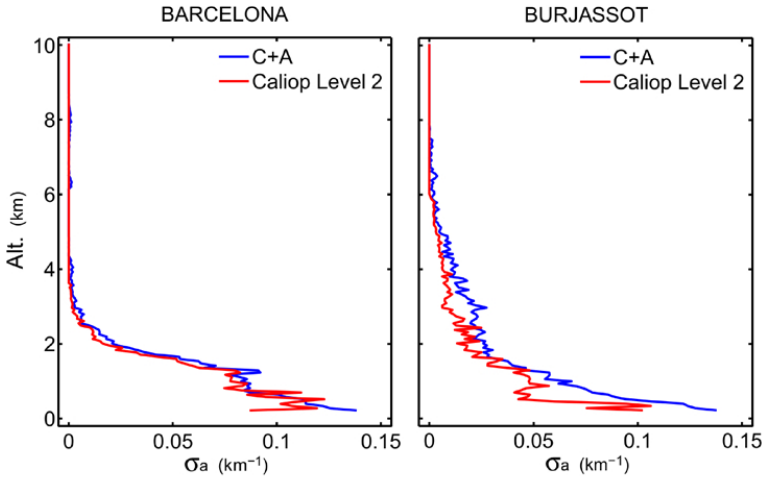

Fig. 13. Mean aerosol extinction profiles for Barcelona (left panel) and Burjassot (right panel) sites. The blue lines are the results obtained with the C + A method, and the red lines the profiles given by CALIOP level 2 data.

AMTD
6, 3983–4038, 2013

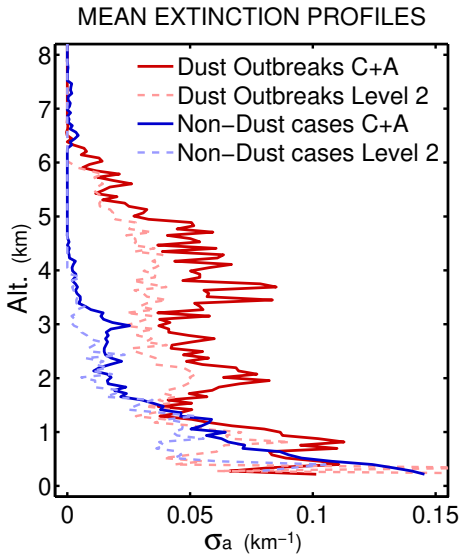

Fig. 14. Mean aerosol extinction profiles for dust outbreaks (red lines) and for the rest of the cases (blue lines). The continuous lines are the C + A results, and the dashed lines are the profiles from CALIOP level 2 data.

AMTD
6, 3983–4038, 2013

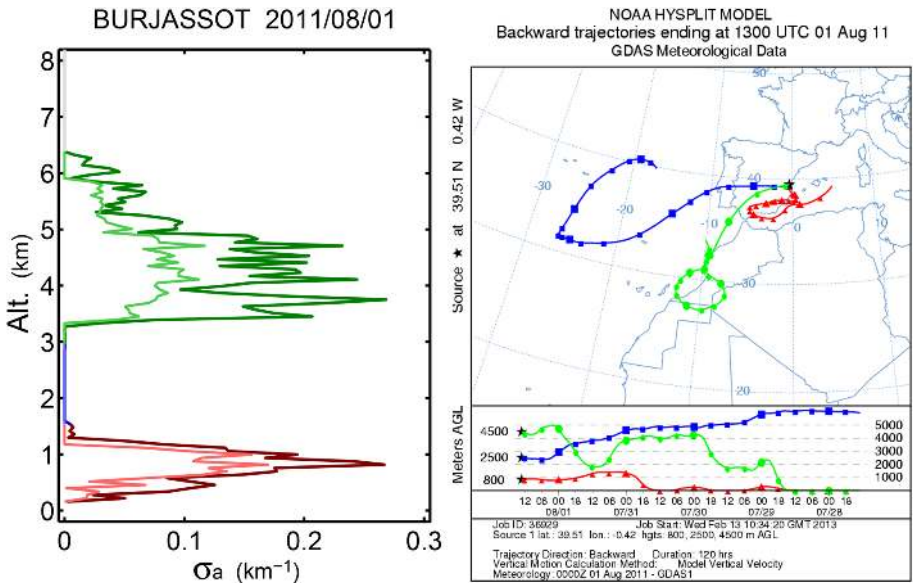

Fig. 15. Left panel: aerosol extinction profile over Burjassot for 1 August 2011. The light thin lines correspond to CALIOP level 2 data, and the thick dark lines are the C + A results. Right panel: HYSPLIT five day air-mass back trajectories at 800 m (red), 2500 m (blue) and 4500 m (green).

AMTD
6, 3983–4038, 2013

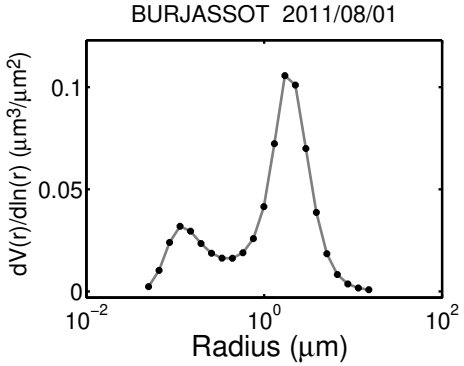

Fig. 16. AERONET derived aerosol size distribution during the dust outbreak on 7 August 2012.

AMTD
6, 3983–4038, 2013

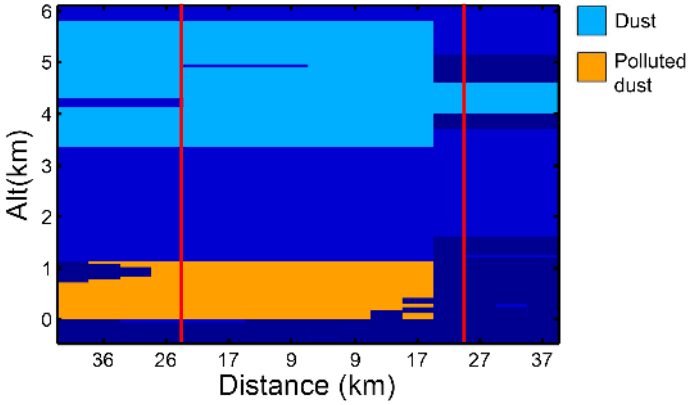

Fig. 17. Aerosol classification near Burjassot according to the CALIOP level 2 algorithms for 1 August 2011. The red lines point the limits of the averaging area.

AMTD
6, 3983–4038, 2013